https://doi.org/10.5194/amt-2020-252
Preprint. Discussion started: 13 July 2020


Atmospheric Measurement Techniques Discussions

# Development of a chemical ionization mass spectrometry system for measurement of atmospheric OH radical

Wei Pu[1]*, Zhouxing Zou[1]*, Weihao Wang[1], David Tanner[2], Zhe Wang[3], and Tao Wang[1]

[1]Department of Civil and Environmental Engineering, The Hong Kong Polytechnic University, Hong Kong, China

[2]School of Earth and Atmospheric Sciences, Georgia Institute of Technology, Atlanta, USA

[3]Division of Environment and Sustainability, The Hong Kong University of Science and Technology, Hong Kong, China

Correspondence to: Tao Wang (cetwang@polyu.edu.hk)

*These authors contributed equally to this work

https://doi.org/10.5194/amt-2020-252
Preprint. Discussion started: 13 July 2020


Atmospheric Measurement Techniques Discussions

**Abstract.** The hydroxyl radical (OH) is the most important oxidant in the atmosphere and plays a central role in tropospheric chemistry. Ambient OH is extremely difficult to measure because of its low concentration and high reactivity. We have developed and optimized a chemical ionization mass spectrometry (CIMS) system to measure OH based on ion-assisted mass spectrometry. A calibration unit was developed based on chemical actinometry to convert detected signals to OH concentration. Different types of ion sources ($^{210}$Po and corona source) and scavenger gases (propane, $C_3F_6$, and $NO_2$) were compared. Radioactive ion source ($^{210}$Po foils) was chosen for lower detection limits, and propane was selected for high elimination efficiency and the negligible influence on the signal stability. The sensitivity of the CIMS instrument to OH radicals is influenced by the efficiencies of titration reaction, ion conversion, and ion transmission. Through adjusting their efficiencies by changing the flow rates and voltages, optimal sensitivity was determined. The background noise from OH interferences was reduced by adjusting the flow rate of scavenger gas. The CIMS system achieved a detection limit of ~0.15 $\times 10^6$ molecules cm$^{-3}$ (signal/noise=2). The CIMS was then taken out to measure ambient OH radicals at an urban site in Hong Kong in April 2019. An obvious diurnal pattern of OH radicals was observed, with the highest concentration of ~$6\times10^6$ molecules cm$^{-3}$ at midday and the lowest concentration of ~$0.25\times10^6$ molecules cm$^{-3}$ at night, with an overall accuracy of about ±51%. The results demonstrated the capability of our CIMS for OH measurements on clear days. The tests and results from our study provide a useful reference to other researchers who wish to develop and apply the CIMS technique to measure OH and other chemicals.

https://doi.org/10.5194/amt-2020-252
Preprint. Discussion started: 13 July 2020


Atmospheric Measurement Techniques Discussions

## 1. Introduction

The hydroxyl radical (OH) is the most important atmospheric cleansing agent and is responsible for the degradation and removal of most of trace gases (Crosley, 1997). In regions strongly affected by anthropogenic activities, reactions of OH with volatile organic compounds (VOCs) and carbon monoxide (CO) lead to the formation of organic peroxy ($RO_2$) and hydroperoxyl ($HO_2$) radicals. They react with NO to form nitrogen dioxide ($NO_2$), producing ozone ($O_3$) (e.g., Hofzumahaus et al., 2009). The reactions of OH with $NO_2$ and sulfur dioxide ($SO_2$) and the self- and cross-reactions of $RO_2$ and $HO_2$ transform the primary pollutants into low-vapor pressure gas molecules such as nitric acid ($HNO_3$), sulfuric acid ($H_2SO_4$), and highly oxidized organic molecules (HOMs) (Lu et al., 2012). In addition, the reaction with OH is the main removal pathway of methane, which is the third most important greenhouse gas. Therefore, OH plays key roles in major environmental issues such as photochemical pollution, acid rain, haze, and climate change (Kulmala et al., 2004; Wang et al., 2017; Calvert et al., 1985; Lu et al., 2019).

The importance of OH in tropospheric chemistry was first recognized by Levy (1971). Since then, concerted efforts have been made to develop techniques to measure OH in the atmosphere (Heard and Pilling, 2003). However, the low concentration, high reactivity, and short lifetime (<1 s) of OH make itself enormously difficult to be detected and quantified. The low concentration requires high sensitivities and small interferences in the instruments; the high reactivity demands a small loss in the ambient sampling, and the short lifetime requires measurement at a high temporal-spatial resolution. It is a huge challenge to meet all of these requirements by a measurement system (Lu et al., 2019).

During the past decades, three major techniques have been developed for in-situ OH measurements: differential optical absorption spectroscopy (DOAS) (Wennberg et al., 1990),

https://doi.org/10.5194/amt-2020-252
Preprint. Discussion started: 13 July 2020


Atmospheric Measurement Techniques Discussions

laser-induced fluorescence (LIF) (Perner et al., 1976), and chemical ionization mass spectrometry (CIMS) (Eisele and Tanner, 1991). DOAS and LIF techniques directly measure OH based on spectroscopic methods. The major advantage of DOAS is that it is self-calibrating via the well-known Beer-Lambert law and thus does not require to separate a calibration device (Heard and Pilling, 2003). DOAS often serves as a primary standard for comparisons with other measurement techniques. However, the application of DOAS to the measurement of ambient OH is limited due to the interferences from other atmospheric constituents (Heard and Pilling, 2003). LIF measures OH by using pulsed 308 nm single photon excitation of OH at low pressure with temporally delayed detection of the resonant OH fluorescence (known as fluorescence assay by gas expansion, FAGE) (Holland et al., 1995), and it requires calibration. The LIF technique has the advantages of direct excitation of OH and good selectivity and sensitivity (Heard and Pilling, 2003). Unlike DOAS and LIF, the CIMS technique measures OH indirectly based on the ion-assisted mass spectrometry method. It employs a chemical reaction scheme that OH is firstly titrated into $H_2SO_4$ and subsequently measured by a specific chem-ionization method (Eisele and Tanner, 1991). CIMS has fewer interference and higher sensitivity compared to either DOAS or LIF techniques for OH measurement because of the higher collection efficiency of ions than photons (Heard and Pilling, 2003). As a result, CIMS processes the lowest detection limit for ambient OH measurement among the three techniques (Heard and Pilling, 2003).

LIF has been the most widely used technique for OH measurement in laboratory and field studies (Stone et al., 2012). However, some LIF instruments may suffer from interferences in environments of rich VOCs and poor NOx. Previous field measurements by LIF in forested regions have observed OH concentrations that are three to five times higher than those predicted by models with presently known OH sources and sinks (McKeen et al., 1997; Lelieveld et al. 2008; Hofzumahaus et al., 2009; Whalley 2011; Lu et al. 2012; Mao et al. 2012;

https://doi.org/10.5194/amt-2020-252
Preprint. Discussion started: 13 July 2020


Atmospheric Measurement Techniques Discussions

Novelli et al. 2014; Feiner et al. 2016; Tan et al. 2017). The disagreements were first attributed to the existence of an unknown source of OH in VOC-rich environment (Peeters et al., 2009; Hofzumahaus et al., 2009), whereas later studies found positive artifacts in some LIF instruments in such environments (Mao et al. 2012; Novelli et al. 2014; Feiner et al. 2016; Liu et al. 2018). For example, Mao et al. (2012) attributed 40-60% observed OH signal at a California forest to interference in their LIF by using a chemical method to remove the interference. Recently, Liu et al. (2018) inferred the equivalent OH concentrations from measurements of isoprene and its oxidation products over Amazon and found that the inferred OH concentrations compared well with the simulated results. On the other hand**,** other groups did not find evidence of the positive bias in their LIF systems, which have different design and configurations, continued to attribute the model underestimated OH to the presence of OH unknown source(s) at their study sites (Whalley 2011; Stone et al., 2012; Fuchs et al.2012; Lu et al. 2012; Tan et al. 2017). It is highly desirable to deploy an alternative technique to re-examine the OH issue in forested regions.

The CIMS technique for measuring OH was first developed at Georgia Institute of Technology by Eisele and Tanner (1991). The system was further improved at National Center for Atmospheric Research by reducing wall reactions (Eisele and Tanner., 1993), by reducing the background signal (Tanner and Eisele., 1995) and by developing a better calibration system (Tanner et al., 1997). Mauldin et al. (1998) modified the CIMS for measurement at an aircraft platform during the First Aerosol Characterization Experiment (ACE1), and Edwards et al. (2003) further upgraded the calibration system. Based on the design of Tanner et al. (1997), another two CIMS instruments were developed at the Meteorological Observatory Hohenpeissenberg, Germany, by Berresheim et al. (2000) and at the National University of Ireland Galway by Berresheim et al. (2013). Kukui et al. (2008) developed a new version of

https://doi.org/10.5194/amt-2020-252
Preprint. Discussion started: 13 July 2020


Atmospheric Measurement Techniques Discussions

the CIMS instrument at the Centre National de la Recherche Scientifique (CNRS), France, which allowed for OH measurements in a moderately polluted atmosphere.

We describe here a new CIMS system that has been tested and optimized at The Hong Kong Polytechnic University (PolyU). The instrument was built at THS, Inc (Atlanta, Georgia) with the same design as the CIMS from the group of Eisele and Tanner. The measurement principles, configurations of the CIMS instrument, and a calibration unit are described in detail. Different scavenger gases, ion sources, and primary ions detection was compared. In addition, the sensitivity and noise of the CIMS instrument to OH radicals were tested by adjusting the flow rates and voltages. Accordingly, their optimal settings were derived. Finally, the test result of ambient OH measurement was presented. These results provide detailed technical information for other researchers who wish to apply the CIMS for ambient OH measurement. To our knowledge, this instrument is the first OH measuring CIMS in Asia.

## 2. Measurement principles

The measurement of hydroxyl radical (OH) in this study was made with a chemical ionization mass spectrometry (CIMS) technique, which has been described previously (Tanner et al., 1997; Sjostedt et al., 2007). Briefly, the ambient OH is titrated to $H_2SO_4$ by adding $SO_2$ into the sample air flow, which initiates the following reaction sequence in the presence of oxygen and water vapor:

$$OH + SO_2 + M \rightarrow HSO_3 + M \quad \text{(R1)}$$

$$HSO_3 + O_2 \rightarrow SO_3 + HO_2 \quad \text{(R2)}$$

$$SO_3 + 2H_2O \rightarrow H_2SO_4 + H_2O \quad \text{(R3)}$$

https://doi.org/10.5194/amt-2020-252
Preprint. Discussion started: 13 July 2020


Atmospheric Measurement Techniques Discussions

However, $H_2SO_4$ in the atmosphere also contributes to the total $H_2SO_4$ concentration. To solve the problem, a scavenger gas is periodically added into the sample air flow to remove OH radicals. Then, $H_2SO_4$ produced from the reaction of OH and $SO_2$ can be obtained:

$$[H_2SO_4]_{OH} = [H_2SO_4]_{TS} - [H_2SO_4]_{BS} \quad \text{(E1)}$$

$[H_2SO_4]_{TS}$ and $[H_2SO_4]_{BS}$ are $H_2SO_4$ concentrations with and without adding scavenger gas, respectively.

Apart from the interference from the pre-existing $H_2SO_4$, the reactions of NO with peroxy radicals ($HO_2$+$RO_2$), whose daytime concentrations are typically 1-2 orders of magnitude of OH, can produce OH in the sample flow (Sjostedt et al., 2007):

$$RO_2 + NO + O_2 \rightarrow R'CHO + HO_2 + NO_2 \quad \text{(R4)}$$

$$HO_2 + NO \rightarrow OH + NO_2 \quad \text{(R5)}$$

Reaction 2 can also produce $HO_2$ radicals as intermediate products. To reduce the positive bias from Reaction 5, another scavenger gas is added into the sample flow after $SO_2$ to scavenge recycled OH radicals.

The $H_2SO_4$ is then converted into $HSO_4^-$ by chemical ionization in reaction with the $NO_3^-$ primary reactant ions:

$$H_2SO_4 + NO_3^- \cdot (HNO_3)_m \cdot (H_2O)_n \rightarrow HSO_4^- \cdot (HNO_3)_m(H_2O)_n + HNO_3 \quad \text{(R6)}$$

$NO_3^- \cdot (HNO_3)_m \cdot (H_2O)_n$ are cluster ions of $NO_3^-$ reactant ions with neutral $HNO_3$ and/or $H_2O$ molecules, with m and n mostly of 0-2 and 0-3 (Berresheim et al., 2000). The $NO_3^- \cdot (HNO_3)_m \cdot (H_2O)_n$ cluster ions are generated by the reaction of $HNO_3$ vapor with electrons (Fehsenfeld et al., 1975):

$$HNO_3 + e^- \rightarrow NO_2^- + OH \quad \text{(R7)}$$

https://doi.org/10.5194/amt-2020-252
Preprint. Discussion started: 13 July 2020


Atmospheric Measurement Techniques Discussions

$$HNO_3 + NO_2^- \rightarrow NO_3^- + HONO \quad (R8)$$

$$NO_3^- + (HNO_3)_m + (H_2O)_n + M \rightarrow NO_3^- \cdot (HNO_3)_m \cdot (H_2O)_n + M \quad (R9)$$

Where $e^-$ is emitted from an ion source. The OH radical (artificial OH) formed from primary ion creation (Reaction 7) is not desirable and regards as noise signal, see details in Section 5.4.3. The $NO_3^- \cdot (HNO_3)_m \cdot (H_2O)_n$ and $HSO_4^- \cdot (HNO_3)_m(H_2O)_n$ are subsequently dissociated by the collisional dissociation chamber (CDC):

$$NO_3^- \cdot (HNO_3)_m \cdot (H_2O)_n + M \rightarrow NO_3^- + (HNO_3)_m + (H_2O)_n + M \quad (R10)$$

$$HSO_4^- \cdot (HNO_3)_m \cdot (H_2O)_n + M \rightarrow HSO_4^- + (HNO_3)_m + (H_2O)_n + M \quad (R11)$$

The OH is finally detected by a mass spectrometer system as $HSO_4^-$ at 97 m/z.

## 3. CIMS system

Figure 1 shows the schematic of our CIMS system, which consists of two parts including a sample inlet system and a mass spectrometer system. The sample inlet system has two regions: chemical titration region and chemical ionization region. The chemical titration region is where $H_2SO_4$ formed by the titration reaction of OH and $SO_2$. Chemical ionization region is for converting $H_2SO_4$ into $HSO_4^-$ ion cluster. The mass spectrometer system consists of three parts including a collisional dissociation chamber (CDC), an ion guide chamber (IGC), and an ion detection chamber (IDC). $HSO_4^-$ ion cluster is dissociated to $HSO_4^-$ in the CDC, then refocused in the IGC and finally detected in the IDC.

### 3.1. Sample inlet

During OH measurements, sample air at ambient temperature and pressure is first drawn into a 5 cm diameter, 32 cm long stainless-steel tube by a blower. The flow velocity is measured manually using a pitot. A scoop is attached to the front of the stainless-steel tube for turbulence reduction. The central part of the flow is then drawn through a 1.6 cm diameter stainless steel

https://doi.org/10.5194/amt-2020-252
Preprint. Discussion started: 13 July 2020


Atmospheric Measurement Techniques Discussions

inlet into the chemical titration region with the flow rate being determined by a mass flow controller (MKS, MFC company). The excess flow is vented back into the atmosphere via an inlet blower.

#### 3.1.1 Chemical titration region

The chemical titration region in Figure 1 is equipped with two pairs of opposed stainless steel needle injectors. The first (front injectors) pair is installed at a 69 mm distance from the tube. The distances between the first and second (rear injectors) pairs are 25.8 mm. To measure OH radicals, $SO_2$ is continuously added into the sample flow from the front injectors to titrate OH into $H_2SO_4$ (Reactions 1-3). In this study, we used $^{32}SO_2$ to titrate OH, and the purity of $SO_2$ is 0.9 vol.%.

As discussed above, atmospheric $H_2SO_4$ can contribute background signals for OH measurements. Therefore, another flow is added through a zero-dead space four-way electrically operated valve, which is automatically switched the injection positions of scavenger gas and pure $N_2$ every 3 minutes (see the pulsed flow in Figure 1). When the scavenger gas is added through the front injectors to the sample flow, $N_2$ is switched through the rear injectors. CIMS is then running in background mode. Under this condition, atmospheric OH simultaneously reacts with $SO_2$ and the scavenger gas, with the reaction of OH with scavenger gas being much faster than $SO_2$. This configuration produces background signal (BS) from the interferences of atmospheric $H_2SO_4$ and the ion source, with negligible contribution from atmospheric OH. When the scavenger gas and $N_2$ are switched into the sample flow through the rear and front injectors, respectively, CIMS is running in the signal mode. Atmospheric OH is all titrated by $SO_2$ and the total signal (TS) is produced. In addition, another flow of scavenger gas is added continuously into the sample flow through the rear injectors to scavenge OH radicals generated from Reaction 5. The OH concentration is obtained

https://doi.org/10.5194/amt-2020-252
Preprint. Discussion started: 13 July 2020


Atmospheric Measurement Techniques Discussions

from the ratio of the difference between the total signal and the background signal to the primary ion ($NO_3^-$) signal. (Tanner and Eisele, 1995):

$$[\mathrm{OH}] = \frac{1}{C} \times \frac{\{\mathrm{HSO_4^-}\}_{\mathrm{TS}} - \{\mathrm{HSO_4^-}\}_{\mathrm{BS}}}{\{\mathrm{NO_3^-}\}} \quad \text{(E2)}$$

Where square brackets and text braces are used to denote concentrations and signal counts, respectively. C is the calibration factor.

### 3.1.2 Chemical ionization region

The sample flow through the chemical titration region is then drawn into the chemical ionization region and mixed with the sheath gas (Figure 1). The sheath gas flow is continuously drawn into the chemical ionization region through the annular space between the 3.5 cm o.d. and 1.2 cm o.d. stainless steel tubes by a diaphragm pump (KNF-813). These tubes are concentric with the downstream end of the chemical titration region. The sheath gas is produced by a zero-air generator (Thermo Electron Corporation, Model 111) attached with active charcoal and silica gel. Therefore, particles, $SO_2$, $NO_x$ and other trace gases are removed effectively from the sheath gas. Before entering the ionization region, $HNO_3$ vapor and the scavenger gas are added continuously to the sheath gas. The $HNO_3$ vapor is obtained by $N_2$ carrier gas flow passing through the headspace of a reservoir of concentrated liquid $HNO_3$. When $HNO_3$ doped sheath gas passes through the ion source (Figure 1), $NO_3^- \cdot (HNO_3)_m \cdot (H_2O)_n$ reactant ions are produced by the reaction of $HNO_3$ and electrons (Reactions 7-9).

The $NO_3^- \cdot (HNO_3)_m \cdot (H_2O)_n$ reactant ions from the sheath gas then react with $H_2SO_4$ molecules from the sample air to form $HSO_4^- \cdot (HNO_3)_m(H_2O)_n$ cluster ions in the chemical ionization region according to Reaction 6. Voltages are added on the sample and sheath flow tubes to produce an electrical field to force the $NO_3^- \cdot (HNO_3)_m \cdot (H_2O)_n$ reactant ions to the center of the chemical ionization region and enhance the interaction of reactant ions with

https://doi.org/10.5194/amt-2020-252
Preprint. Discussion started: 13 July 2020


Atmospheric Measurement Techniques Discussions

$H_2SO_4$. This effectively increases the signal levels and improves the sensitivity for OH measurements.

The total flow (Figure 1) is then exhausted at the end of the chemical ionization region through diaphragm pumps (Thomas, SK-668) and controlled by an MFC. To prevent the $HNO_3$ vapor from corroding the pump and MFC and polluting the ambient air, the exhaust flow is first filtered through active charcoal cartridges and then vented back into the atmosphere at a distance of >10 m from the sampling point. A small portion of the total flow is finally drawn into the mass spectrometer system through a 101.6 um diameter pinhole. The air molecules, especially $H_2O$ molecules may form higher-order clusters upon adiabatic expansion and cool in the vacuum mass spectrometer system (Berresheim et al., 2000). To reduce this influence, a small counterflow of $N_2$ buffer gas is added on the atmospheric pressure side of the pinhole (Figure 1). And voltages are added at the positions of $N_2$ buffer and pinhole to force the ions into the mass spectrometer system.

### 3.2. Mass spectrometer system

The mass spectrometer system is separated into three differentially pumped chambers with two adjacent chambers being connected through a 4 mm pinhole (Figure 1). The first chamber behind the pinhole is a collisional dissociation chamber (CDC). The pressure of the CDC is typically maintained at around 0.5 hPa through a drag pump (Adixen, MDP 5011) and a scroll pump (Agilent Technologies, IPD-3). The CDC has a high ion kinetic energy (i.e. high electric field to number density ratio), and most of the entered cluster ions (e.g. $HSO_4^- \cdot (HNO_3)_m(HO_2)_n$ and $NO_3^- \cdot (HNO_3)_m \cdot (HO_2)_n$ ) are dissociated in the CDC through Reactions 10-11.

The second chamber is an octopole ion guide high vacuum chamber (IGC). In this chamber, the pressure is maintained at about $1.3 \times 10^{-3}$ hPa through a turbo molecular pump (Agilent

https://doi.org/10.5194/amt-2020-252
Preprint. Discussion started: 13 July 2020


Atmospheric Measurement Techniques Discussions

Technologies, TwisTorr 304 Fs) and the same scroll pump. Here, the ions from the CDC are refocused by an octopole ion guide and transported to the third chamber.

The third chamber (IDC) contains a quadrupole mass filter and detector with attached signal amplifier electronics. The mass-selected ions of the quadrupole are amplified and detected by a channeltron ion multiplier, and then counted based on standard techniques (Sjostedt et al., 2007). This chamber maintains a pressure of about $2.6 \times 10^{-5}$ hPa through another turbo molecular pump (Agilent Technologies, TwisTorr 304 Fs) and the same scroll pump.

## 4. Calibration

### 4.1 Calibration principle

The calibration of CIMS (Figure 2a) is achieved by controlled concentrations of OH radicals, which is produced through photolysis of water vapor by 184.9 nm light (Tanner and Eisele, 1995):

$$H_2O + h\nu\ (184.9\ \text{nm}) \rightarrow OH + H \qquad \text{(R12)}$$

$$H + O_2 + M \rightarrow HO_2 + M \qquad \text{(R13)}$$

The calibration factor C is then determined based on the produced OH concentrations and detected signals of $HSO_4^-$ and $NO_3^-$ according to Equation 2.

### 4.2 Calibration unit

Figure 2 shows the main components of the calibration unit. The length of the cuboid stainless steel tube is 52 cm with 1.6 cm side length. A high-precision capacitance humidity measurement hygrometer (Vaisala, HMP100) is connected at the front of the tube and is used to measure the temperature $T$ and dew point temperature $T_d$ of the mixed air. The optical elements for illumination are mounted at the end of the tubes (air outlet side) to minimize the

https://doi.org/10.5194/amt-2020-252
Preprint. Discussion started: 13 July 2020


Atmospheric Measurement Techniques Discussions

influence of wall loss during calibration. The optical elements consist of a Pen Ray mercury lamp (Analytik Jena, UVP Pen Ray) and a bandpass filter. The bandpass filter blocks most of the photons emitted from the Hg lamp except those at 184.9 nm. A small $N_2$ flow is purged to prevent UV absorption and the formation of ozone (Kukui et al., 2008). Finally, the transmitted light enters the tube and photolyzes water vapor to produce OH radicals according to Reaction 12. The mixing ratio of water vapor in the air flow is controlled through the mix of the dry synthetic air and humidity air from a water bubbler.

### 4.3 Calibration quantification

#### 4.3.1 OH quantification

The concentrations of OH radicals produced from the water vapor photolysis reaction can be described as follow:

$$[\mathrm{OH}] = I \times t \times \sigma_{\mathrm{H_2O}} \times \phi_{\mathrm{H_2O}} \times [\mathrm{H_2O}] \quad \text{(E3)}$$

Where $I$ and $t$ are the photon intensity (unit: photons $s^{-1}$ $cm^{-2}$) and the reaction time of $H_2O$ photolysis, respectively. [OH] and [$H_2O$] are the concentrations of OH radicals and water vapor, respectively, $\sigma_{\mathrm{H_2O}}$ is the photolysis cross-section of water vapor at 184.9 nm ($7.22\times10^{-20}$ $cm^2$, Cantrell et al., 1997 ) and $\phi_{\mathrm{H_2O}}$ represents the photolysis quantum yield, which is assumed to be 1.0 at 184.9 nm. [$H_2O$] is calculated according to the temperature (T), saturated water vapor pressure ($P^{\circ}_{H_2O}$) and relative humidity (RH) of the mixed air flow:

$$[\mathrm{H_2O}] = \frac{RH \times P^{\circ}_{H_2O} \times 100}{RT} \times NA \quad \text{(E4)}$$

R is the ideal law constant and NA is the Avogadro's number. $I$ and $t$ are obtained as a combined product $It$.

#### 4.3.2 *It* quantification

https://doi.org/10.5194/amt-2020-252
Preprint. Discussion started: 13 July 2020


Atmospheric Measurement Techniques Discussions

The combined product *It* is obtained based on the chemical actinometry method (Figure 2b). This method measures $NO_x$ generated from $N_2O$ photolysis with the same calibration unit under the same condition of the CIMS calibration. Since $N_2O$ photolysis generates $NO_x$ through the illumination of the UV light with the same photon intensity as the $H_2O$ photolysis, product *It* can be determined by measured $NO_x$ and $N_2O$ mixing ratios (Edwards et al., 2003).

Briefly, high purity $N_2O$ (99.9%) mixed with dry $N_2$ or dry synthetic gas flows into the calibration unit. The photolysis of $N_2O$ leads to the formation of $NO_x$ in the presence of oxygen and nitrogen through the following reactions (Edwards et al., 2003):

$$N_2O + h\nu\ (184.9\ \text{nm}) \rightarrow N_2 + O(^1D) \quad \text{(R14)}$$

$$O(^1D) + O_2 \rightarrow O(^3P) + O_2 \quad \text{(R15)}$$

$$O(^1D) + N_2 \rightarrow O(^3P) + N_2 \quad \text{(R16)}$$

$$O(^3P) + O_2 + M \rightarrow O_3 + M \quad \text{(R17)}$$

$$O(^1D) + N_2O \rightarrow 2NO \quad \text{(R18)}$$

$$O(^1D) + N_2O \rightarrow N_2 + O_2 \quad \text{(R19)}$$

The $O_3$ produced from Reaction 17 could oxidize NO to $NO_2$. Therefore, the photolysis of $N_2O$ eventually converts it to $NO_x$ which is concurrently measured by a commercial $NO_x$ detector (Thermo, Model 42i-TL) by converting $NO_2$ to NO with a blue light converter and NO being measured by the chemiluminescence technique. The combined product *It* is a function of the mixing ratios of $N_2O$, $N_2$, $O_2$, and produced $NO_x$:

$$It = \frac{(K_{15} \times [O_2] + K_{16} \times [N_2] + (K_{18} + K_{19}) \times [N_2O]) \times [NO_X]}{2 \times K_{18} \times \sigma_{N_2O} \times \phi_{N_2O} \times [N_2O]^2} \quad \text{(E5)}$$

https://doi.org/10.5194/amt-2020-252
Preprint. Discussion started: 13 July 2020


Atmospheric Measurement Techniques Discussions

where $K_{15}$, $K_{16}$, $K_{18}$, $K_{19}$ are the rate constants of Reaction 15, 16, 18 and 19, respectively, whose values can be found elsewhere (Kurten et al., 2012). $\sigma_{N_2O}$ is the absorption cross-section of $N_2O$ ($1.43\times10^{-19}$ $cm^2$, Kurten et al., 2012) and $\phi_{N_2O}$ is the photolysis quantum yield which is assumed to be 1.0 (Kurten et al., 2012).

Ideally, the $N_2O$ actinometry experiment should be conducted with the same flow rate as in water vapor photolysis experiment such that the reaction time of these two photolysis experiments can be the same. However, at the flow rate suitable for CIMS calibration (10 slpm), the concentration of $NO_x$ produced from $N_2O$ photolysis is close to the detection limit of the $NO_x$ detector. Hence, the $N_2O$ actinometry experiment was carried out at a lower flow rate (3 and 6 slpm) to increase reaction time for photolysis and then the $NO_x$ production. The *It* values for $N_2O$ photolysis experiment $(It_{N_2O})$ and water vapor photolysis experiment $(It_{H_2O})$ have the following relationship:

$$It_{H_2O} = \frac{FR_{N_2O} \times It_{N_2O}}{FR_{H_2O}} \quad \text{(E6)}$$

where $FR_{N_2O}$ and $FR_{H_2O}$ represent the flow rate for the experiment of $N_2O$ photolysis and water vapor photolysis, respectively. Based on this equation, $It_{H_2O}$ can be obtained by scaling $It_{N_2O}$ with the ratio of $FR_{N_2O}$ and $FR_{H_2O}$. The relation in Equation 6 between the product *It* and flow rate is validated in the next section.

#### 4.3.2 *It* determination

Figure 3 shows the results of $N_2O$ actinometry experiment. Figure 3a shows the $NO_x$ produced as the function of $N_2O$ mixing ratios from 10% to 15% at different flow rates ($FR_{N_2O}$ = 3, 6, and 10 slpm). Generally, increasing $N_2O$ led to more production of $NO_x$, and the lower flow rate resulted in longer reaction time and the higher $NO_x$ concentrations. In figure 3b, the product *It* respect to different flow rate was calculated according to E5 based on the produced

https://doi.org/10.5194/amt-2020-252
Preprint. Discussion started: 13 July 2020


Atmospheric Measurement Techniques Discussions

$NO_x$ and $N_2O$ result in Figure 3a. The product *It* linearly increased with the inverse of the flow rate, which validates the linear dependency between product *It* and inverse of the flow rate shown by E6. This linear depend is consistent with a previous study (Kurten et al., 2012). In addition, the product *It* was mostly independent on $N_2O$ mixing ratios with variation from 10% to 15%. Figure 3c shows the flow rate scaled product *It* as a function of different $N_2O$ mixing ratio. Based on the E6, the flow rate scaled product *It* ($It_{H_2O}$) is calculated from $It_{N_2O}$ in Figure 3b multiplying the ratio of $FR_{N_2O}$ (3, 6, and 10 slpm, respectively) to $FR_{H_2O}$ (10 slpm). The flow rate scaled product *It* variate from 1.37 to 1.53 x $10^{11}$ at different flow rates and $N_2O$ mixing ratio. As a result, the value of $It_{H_2O}$ was derived as 1.46 x $10^{11}$ photon $cm^{-1}$ from the average of flow rate scaled product *It*.

### 4.3.3 Calibration result

Figure 4 shows an example of a typical procedure for determining the calibration factor. The instrument signals were continuously measured by adjusting $H_2O$ concentrations without changing other parameters. The different OH concentrations were calculated according to Equation 3. For each step, the signal intensities (in Hz) of $HSO_4^-$ and $NO_3^-$ were collected for 6 minutes with background mode and signal mode of each 3 minutes. The calibration factors were determined from the calculated OH concentrations and signal intensities based on Equation 2. The red dots in Figure 4 represent the average calibration factors for every 3 minutes. The result shows that the calibration factors for different steps were very close from 1.60 to 1.69x$10^{-10}$ and were independent of water vapor concentrations, which indicates the high performance of calibration quantification. Then, the averaged calibration factor for our CIMS is 1.64 x$10^{-10}$ molecule/$cm^{-3}$.

## 5. Optimizations of instrument performance

https://doi.org/10.5194/amt-2020-252
Preprint. Discussion started: 13 July 2020


Atmospheric Measurement Techniques Discussions

As shown in Figure 1, the CIMS system is complicated, and its performance is determined by different parameters and components. In order to improve the performance of the CIMS for OH measurement, different types of ion sources ($^{210}$Po radioactive ion source, corona source), scavenger gases (propane, $C_3F_6$, and $NO_2$), and primary ions detection were compared. Moreover, the instrument sensitivity and noise were optimized by adjusting the flow rates and voltages.

### 5.1. Ion source

Radioactive ion source ($^{210}$Po or $^{241}$Am) and corona discharge source (corona ionizer) were generally used as the ion source in previous studies (Berresheim et al., 2000; Sjostedt et al., 2007; Kukui et al., 2008). In this study, $^{210}$Po and corona sources were compared.

#### 5.1.1 $^{210}$Po

The $^{210}$Po acts as an ion source through the alpha decay. Briefly, $^{210}$Po emitted alpha particles that interact with the carrier gas to quickly form thermalized electrons and positive ions (Fehsenfeld et al., 1975). The formed electrons react with $O_2$ and then $HNO_3$ to produce $NO_3^- \cdot (HNO_3)_m \cdot (H_2O)_n$ reactant ions for ion conversion. Radioactive ion source such as $^{210}$Po was usually used due to the low OH interference and convenience of installation. We compared $^{210}$Po ions source and corona source (see below) for the performance on OH measurements (Figure S1). The result showed that the detection limit by $^{210}$Po ions source was lower than the corona source. In this study, $^{210}$Po foils were chosen as the ion source in our CIMS system. We note that the radioactive ion source is usually subject to stringent health safety regulations and the users should apply a permit to use the radioactive source. In addition, $^{210}$Po is an isotope of polonium and undergoes alpha decay to stable $^{206}$Pb with a half-life of about 140 days. Therefore, in order to keep stable signal intensities for primary ions, $^{210}$Po foils need to be replaced regularly.

https://doi.org/10.5194/amt-2020-252
Preprint. Discussion started: 13 July 2020


Atmospheric Measurement Techniques Discussions

### 5.1.2 Corona source

Corona ionizer generates $NO_3^-$ by the discharge formed between the tungsten needle and a 1 mm diameter plate 3 mm from the needle tip (Kukui et al., 2008). Corona source has the advantage of producing much higher concentrations of $NO_3^- \cdot (HNO_3)_m \cdot (H_2O)_n$ primary ions compared with radioactive $^{210}$Po or $^{241}$Am foils, which leads to higher concentrations of $HSO_4^-$ and higher signal intensities (higher sensitivities). However, the corona discharge source is known to produce a significant amount of neutral species including OH radicals. When using the corona discharge source in our CIMS instrument, the concentrations of produced OH artifacts were much higher than those found in the ambient atmosphere (Figure S1). Although scavenger gas added in the sheath flow can remove most artificial OH radicals, the remaining interferences are still comparable with those in ambient environments and can deteriorate the detection limit of the CIMS instrument for OH measurements.

## 5.2 Scavenger gas

As discussed in Section 3, scavenger gas is very important for determining the performance of OH measurement by CIMS. Three types of scavenger gas (propane, $C_3F_6$, and $NO_2$) have been used in previous studies by different groups (Berresheim et al., 2000; Sjostedt et al., 2007; Kukui et al., 2008). However, there have been no reports on comparisons of these three scavenger gases. In this study, they were tested in the laboratory. A scavenger gas was added in two positions for different purposes. In the sheath flow, the scavenger gas reduced the interference of OH artifacts from the ion source; in the sample flow, it was injected to eliminate the ambient OH to determine background.

### 5.2.1 Propane

For propane, 99.95 vol.% pure propane (purchase from the Harvest Wise Gases (H.K.) Company) added in sheath flow could effectively (~80% see Figure 6) remove artificial OH

https://doi.org/10.5194/amt-2020-252
Preprint. Discussion started: 13 July 2020


Atmospheric Measurement Techniques Discussions

radicals from the ion source, and the remaining contributed a low and stable signal intensity at 97 m/z. For the OH removal efficiency of propane in sample air, even at OH concentrations of two orders of magnitude higher than ambient OH level, propane could remove OH at 97.7% (for more details, see Section 5.4.3). In addition, the signal intensity of the primary ions was not affected by the added propane and kept stable (Figure S2). Propane is cheap and easy to purchase. In our CIMS system, propane was selected as the scavenger gas.

#### 5.2.2 $C_3F_6$

For $C_3F_6$, although its OH removal efficiency was high enough, it was found to suppress the signal intensities detected by the mass spectrometer system. With no $C_3F_6$, the signal intensity at 64 m/z for primary ions was quite stable even within one month. However, once $C_3F_6$ was added, the signal intensity at 64 m/z declined quickly as shown in Figure S2. As a result, the sensitivity for OH measurements decreased and the detection limit increased. Initially, we suspected that the purchased $C_3F_6$ cylinder gas had high impurities, which may consume $NO_3^-$ ions. But, after replacing three different $C_3F_6$ cylinders gas which was purchased from two different suppliers, the problem remained. We suspect that $C_3F_6$ may suppress the ion detection efficiency of the mass spectrometer system.

#### 5.2.3 $NO_2$

$NO_2$ was found not only to remove OH radicals but also to $HO_2$ radicals by converting them into $HO_2NO_2$ when NO was present in sample air. This means that compared to the other scavenger gases, $NO_2$ provides a better measurement accuracy, especially in a high NO environment. However, only 1.0 vol.% $NO_2$ cylinder gas was available for our experiment due to restrictions of using higher concentrations of $NO_2$, and its removal efficiency was not high enough to remove OH. We note that high purity $NO_2$ gas is very dangerous and must be handled with extreme caution.

https://doi.org/10.5194/amt-2020-252
Preprint. Discussion started: 13 July 2020


Atmospheric Measurement Techniques Discussions

### 5.3 Primary ions detection

Determination of the concentrations of OH radicals need to use the signal intensities of $NO_3^-$ ions according to Equation 2. In our study, $NO_3^-$ primary ions are detected by the mass spectrometer system at 64 m/z. Some studies traced the $NO_3^-$ ions based on the signal intensities at 62 m/z (Tanner et al., 1997). However, we noticed that the concentrations of $NO_3^-$ produced in the inlet system are extremely high. Even though a small portion of the $NO_3^-$ ions are finally detected by the mass spectrometer system, they can yield very strong signal intensities. After operating the CIMS instrument with detecting the signal of $NO_3^-$ ions at 62 m/z about half a year, we found a significant decrease in the signal intensity at 62 m/z (with all instrument settings unchanged), which may be due to the accelerated aging of the channeltron detector by the high $NO_3^-$ ions concentrations. Therefore, the isotopic signal ($N^{18}O_3^-$)at 64 m/z was chosen to detect $NO_3^-$ primary ions for extended operation. The signal intensity at 64 m/z is lower than at 62 m/z by about a factor of 167 (Kurten et al., 2012).

### 5.4 Instrument sensitivity and noise

#### 5.4.1 Parameters influencing the sensitivity

The sensitivity (S) of the CIMS instrument to the OH radicals dependent on the reaction efficiency of OH and $SO_2$ in chemical titration region (f(RE)), the conversion efficiency of $H_2SO_4$ to $HSO_4^-$ in chemical ionization region (f(CE)), and the transmitted efficiency of $HSO_4^-$ from sample inlet to mass spectrometer system (f(TE)):

$$S \sim f(RE) \cdot f(CE) \cdot f(TE)$$

f(RE) is dependent on the reaction time and the reaction rate, which is mainly related to the velocity of sample air flow and the concentration of $SO_2$. f(CE) is mainly controlled by the mixing of $H_2SO_4$ in sample flow and $NO_3^- \cdot (HNO_3)_m \cdot (HO_2)_n$ primary ions in sheath flow in

https://doi.org/10.5194/amt-2020-252
Preprint. Discussion started: 13 July 2020


Atmospheric Measurement Techniques Discussions

the chemical ionization region, which is not only dependent on the mixing of sample flow and sheath flow but also the voltages on the flow tubes as discussed in Section 3.1. f(RE) is related to the $N_2$ buffer gas flow and voltages. We can optimize the sensitivity (S) by adjusting the $SO_2$ flow, sample/sheath flows, $N_2$ buffer gas flow, and voltages.

### 5.4.2 Sensitivity optimization

#### 5.4.2.1 Optimization of $SO_2$ gas flow

Figure 5a shows the normalized signal intensity (NSI) at 97 m/z for $HSO_4^-$ as a function of the flow rate of $SO_2$ (0.9 vol.%). The NSI first increased with increased $SO_2$. Then, the NSI became independent of the added $SO_2$ amount and a stable signal was obtained with flow rate > ~2.5 sccm. We set the $SO_2$ flow rate 5 sccm for a factor of 2 margin sccm for our operation, following the previous study (Sjostedt et al., 2007).

#### 5.4.2.2 Optimization of sample/sheath flow

Figure 5b shows the NSI as a function of the ratio of sample flow to sheath flow. The NSI firstly increased and then decreased with the increased ratio, with a peak value at a sample/sheath flow ratio of 0.3. This ratio was independent of the sample flow rates from 12 to 21 slpm. We think that this ratio produced a turbulent total flow in the chemical ionization region, facilitating a fast mixing of the reactants, enhancing the ionization efficiency of $H_2SO_4$, and increasing NSI at 97 m/z. (Tanner and Eisele, 1995; Tanner et al., 1997).

The effects of the sample flow rate on NSI are shown in Figure 5c. The ratio of sample to sheath flow was fixed as 0.3. Briefly, the NSI increased with the decreased flow rate. The result is expected as the lower the sample flow rate is, the longer times Reactions 1-3, as well as Reaction 6, have, which improves both f(RE) and f(CE). However, the increased reaction time of Reactions 1-3 will increase the OH interference produced from the $HO_2$ recycling in the presence of NO in sample air. Previous studies usually kept the reaction time less than 60 ms

https://doi.org/10.5194/amt-2020-252
Preprint. Discussion started: 13 July 2020


Atmospheric Measurement Techniques Discussions

(e.g. Tanner et al., 1997). After considering these two factors, the sample and sheath flow rates were set at 3.7 and 12.6 slpm, respectively, which gives a reaction time of ~47 ms. The optimal f(RE) is determined.

#### 5.4.2.3 Optimization of voltages

Figure 5d-e shows the effects of voltages on NSI. As mentioned above, the voltages are applied to force the ions to the centre of the chemical ionization region and enhances the ionization efficiency. Similar to the flow ratio, the increase of voltage difference (inlet voltage minus sheath voltage) firstly increased the NSI and then decreased it (Figure 5d). At the voltage difference of 48 V, the peak NSI was achieved. In Figure 5e, the NSI increased with the negative sheath voltage and then kept stable with sheath voltage < -70V (the voltage difference was fixed as 48 V). based on these results, we set the inlet and sheath voltages at -32 and -80 V, respectively. At these settings, the optimal f(CE) was determined. The cross interactions of sample/sheath flow and voltages on NSI were also evaluated in Figure S3. The highest NSI was achieved when the sample/sheath flow ratio was close to 0.3 for different voltages. This result indicates the response of NSI on voltages is relatively stable at the flow ratio of 0.3. The voltages added to the pinhole also force the ion to the central of pinhole and pass through it which are set at -70 and -40V.

#### 5.4.2.4 Optimization of $N_2$ buffer gas flow

Generally, the mass flow into the mass spectrometer system is fixed and the $N_2$ buffer gas just changes the amount of sample air versus dry $N_2$. Figure 5f shows the effect of $N_2$ buffer gas flow. Generally, the NSI increased with the decreased flow rate since more ions in sample air entered the mass spectrometer system and further increased the f(TE). However, a lower flow rate of $N_2$ buffer gas also makes more neutral molecules in sample air entering the mass

https://doi.org/10.5194/amt-2020-252
Preprint. Discussion started: 13 July 2020


Atmospheric Measurement Techniques Discussions

spectrometer system and influencing the instrument (Berresheim et al., 2000). Therefore, the flow rate of $N_2$ buffer gas was set as 440 sccm, and the optimal f(TE) was determined.

### 5.4.3 Noise minimization

As discussed above, the instrument noises for OH measurements are from $H_2SO_4$ in ambient air and OH produced by the ion source. These noises can be reduced by adding a scavenger gas.

In order to minimize the artificial OH produced by ion source, the scavenger gas was added to sheath flow. Figure 6 shows the signal intensity at 97 m/z where $N_2$ gas was used as sample air so that there were no OH radicals in sample air. The artificial OH signal from the $^{210}Po$ ion source was ~$3.5\times10^6$ molecules $cm^{-3}$ without propane in sheath gas, which is comparable to the typical OH concentrations in ambient environments. When propane was added into the sheath gas, the artificial signals were effectively reduced to less than ~$1\times10^6$ molecules $cm^{-3}$ and kept stable when the flow rate was higher than 1 sccm. Based on the result, we set a flow rate of 2 sccm for propane in the sheath flow.

To quantify and subsequently remove the contribution of ambient $H_2SO_4$ to signal at 97 m/z, the scavenger gas was switched to the front injector to eliminate all ambient OH for the detection of ambient $H_2SO_4$ signal only. The OH removal efficiency (RE) of the scavenger gas in sample flow can influence the instrument's performance. Figure 7 shows the RE of propane added in the sample flow. Excessive OH radical compared to ambient levels were produced from the OH calibration source. The RE increased with the increased propane flow rate initially and started to level off when more propane was added. We adopt the flow rate of propane at 2 sccm in front injector (also in rear injector), which led to~98% removal efficiency for OH and allowed quantification of ambient $H_2SO_4$ for subsequent noise subtraction (E2).

## 6. Detection limit and uncertainty

https://doi.org/10.5194/amt-2020-252
Preprint. Discussion started: 13 July 2020


Atmospheric Measurement Techniques Discussions

The detection limit can be calculated as follows,

$$DL = \frac{1}{C} \times \frac{n * \sigma}{\{NO_3^-\}} \quad \text{(E7)}$$

Where DL is the detection limit in $10^6$ molecule/cm$^3$, C is the calibration factor, and *n* is the ratio of signal to noise S/N. σ represents the standard deviation of the signal intensity of $HSO_4^-$ at 97 m/z, and $\{NO_3^-\}$ represents the signal intensity of $NO_3^-$ at 64 m/z at the integration time t.

Figure 8 shows the concentrations of OH radicals and the corresponding detection limit (S/N=2, average time=6 minutes) in the laboratory. The detection limit was quite stable over the whole day and ranged from 0.08 to 0.20*$10^6$ molecule cm$^{-3}$, with an average value of approximately 0.15 *$10^6$ molecule cm$^{-3}$.

The uncertainty for the calibration factor (C) of OH measurements is dependent on the uncertainties of all the parameters involved in the calculation of the concentrations of OH radicals and the precision of the measurements of signal at 64 m/z and 97 m/z. The uncertainty was ~36% for *It* (see Figure 3), $\sigma_{H_2O}$~5% for $\sigma_{H_2O}$, <1% for $\phi_{H_2O}$ (Cantrell et al. 1997), and ~10% for the water concentration (Kukui et al., 2008). The precision of the measurements signal at 64 m/z and 97 m/z of the CIMS instrument (2σ) was 11% (for 6 min integration time). The overall uncertainty for the calibration factor was about 38%.

## 7. Field deployment of CIMS

In order to examine the performance of our CIMS in the ambient environment, we deployed the optimized instrument to an urban site of Hong Kong in April 2019 (Figure S4). The site was located on the 11$^{th}$ floor of a teaching building on the campus of The Hong Kong Polytechnic University (PolyU) and was surrounded by several busy roads. The sample inlet was positioned horizontally facing the south. Measurements were made with a time resolution of 10 seconds. A typical measurement sequence consisted of 3 minutes in the background mode

https://doi.org/10.5194/amt-2020-252
Preprint. Discussion started: 13 July 2020


Atmospheric Measurement Techniques Discussions

and 3 minutes in the signal mode. Figure 9a shows the diurnal profile of OH concentrations (3-minute average) observed on April 25, 2019, and the solar radiation measured using UTA-LI200 at a time resolution of 1 minute. Figure 9b shows the measured signal intensities at 97 m/z at the signal mode and the background mode. The OH concentrations exhibited a clear diurnal profile with the highest value of ~$6\times10^6$ molecules $cm^{-3}$ at midday and the lowest level of ~$0.25\times10^6$ molecules $cm^{-3}$ at night. The OH concentrations were highly correlated to solar radiation, which was similar to previous studies (e.g. Rohrer and Berresheim, 2006; Tan et al., 2017). The 3-minute average OH concentrations were above the detection limits ($0.5\text{-}2\times10^6$ molecules $cm^{-3}$) most of the daytime, except during a cloudy period (08:00 to 10:00) (Figure 9a). This preliminary result demonstrated the capability of our CIMS for measuring ambient OH on a clear day in an urban environment. However, Figure 9b reveals that the contribution to instrument background from ambient $H_2SO_4$ was significant at the site, which raised the detection limit and measurement uncertainty (to 51%). Future work will make use of isotopically labelled $^{34}SO_2$ to eliminate $H_2SO_4$ interference.

## 8. Summary and conclusions

To measure the atmospheric OH radicals, we have developed the first chemical ionization mass spectrometry (CIMS) system in Asia. It is an indirect measurement technique that converts OH radicals to $HSO_4^-$ which is detected by the ion-assisted mass spectrometry method. In addition, the calibration system has been developed. A series of comparisons of different ion sources, scavenger gases, and primary ions detection have been conducted to optimize the performance of the CIMS for OH measurement. The sensitivity is dependent on the efficiencies of titration reaction, ion conversion, and ion transmission which have been improved by optimizing the flow rates of a myriad of gases and voltages in various components. An initial field test has demonstrated the capacity of this instrument in measuring ambient OH in an urban site on clear days. The main findings on the key parameters are summarized below.

https://doi.org/10.5194/amt-2020-252
Preprint. Discussion started: 13 July 2020


Atmospheric Measurement Techniques Discussions

(1) $^{210}Po$ has lower artificial OH interference compared to a corona ionizer, and it is adopted as the ion source.

(2) $C_3H_8$ is a better OH scavenger than $C_3F_6$ and $NO_2$ (low concentration) because of the high elimination efficiency and signal stability of $C_3H_8$.

(3) A procedure has been developed to optimize the flow rates of sample gas, sheath gas, and $N_2$ buffer gas, voltages on the sample inlet system and the concentration of $SO_2$ titration gas with the aim to increase instrument's sensitivity and reduce noise.

(4) The CIMS instrument achieved a detection limit of $0.15\times10^6$ molecules $cm^{-3}$ and uncertainty of 38% (S/N=2) under laboratory conditions. In the field, the detection limit increased to about $0.15 \times 10^6$ molecules $cm^{-3}$ on clear days, with the overall accuracy of about 51%.

(5) Future work includes more field experiments in various environments and utilization of isotopically labelled $^{34}SO_2$ to eliminate the $H_2SO_4$ interference.

We note that the optimal values of instrument parameters may differ in different CIMS systems due to the different design and/or configurations, the test procedures and results from our study provide a useful reference to other researchers who wish to apply CIMS technique to measure atmospheric OH radicals.

https://doi.org/10.5194/amt-2020-252
Preprint. Discussion started: 13 July 2020


Atmospheric Measurement Techniques Discussions

**Data availability.** All data used to produce this study can be obtained by contacting Tao Wang (cetwang@polyu.edu.hk)

**Supplement.** The supplement related to this article is available on line at:

**Author contribution.** TW invited the project, WP and ZZ designed and performed experiments with contributions from WW, ZW, DT and TW. WP, ZZ, and TW write the paper with contributions from DT and ZW.

**Competing interests.** The authors declare that they have no conflict of interest.

**Acknowledgments**

We thank the Environmental Protection Department of Hong Kong for loaning the CIMS instrument.

**Financial support.** This research was financially supported by the Hong Kong Research Grants Council (T24-504/17-N and A-PolyU502/16)

**Reference:**

Berresheim, H., Elste, T., Plass-Dülmer, C., Eisele, F. L. and Tanner, D. J.: Chemical ionization mass spectrometer for long-term measurements of atmospheric OH and H2SO4, Int. J. Mass Spectrom., 202(1–3), 91–109, doi:10.1016/S1387-3806(00)00233-5, 2000.

Berresheim, H., McGrath, J., Adam, M., Mauldin, R. L., Bohn, B., & Rohrer, F. (2013). Seasonal measurements of OH, NOx, and J(O1D) at Mace Head, Ireland. Geophysical Research Letters, 40(8), 1659–1663. https://doi.org/10.1002/grl.50345

Calvert, J. G., Lazrus, A., Kok, G. L., Heikes, B. G., Walega, J. G., Lind, J. and Cantrell, C. A.: Chemical mechanisms of acid generation in the troposphere, Nature, 317(6032), 27–35, doi:10.1038/317027a0, 1985.

Cantrell, C. A., Zimmer, A. and Tyndall, G. S.: Absorption cross sections for water vapor from 183 to 193 nm, Geophys. Res. Lett., 24(17), 2195–2198, doi:10.1029/97GL02100, 1997.

Crosley, D. R.: 1993 Tropospheric OH Photochemistry Experiment: A summary and perspective, J. Geophys. Res. Atmos., 102(5), 6495–6510, doi:10.1029/96jd03324, 1997.

Edwards, G. D., Cantrell, C. A., Stephens, S., Hill, B., Goyea, O., Shetter, R. E., Mauldin, R. L., Kosciuch, E., Tanner, D. J., & Eisele, F. L. (2003). Chemical Ionization Mass Spectrometer Instrument for the Measurement of Tropospheric HO2 and RO2. *Analytical Chemistry*, *75*(20), 5317–5327. https://doi.org/10.1021/ac034402b

Eisele, F. L. and Tanner, D. J.: Ion-assisted tropospheric OH measurements, edited by Intergovernmental Panel on Climate Change, J. Geophys. Res., 96(D5), 9295–9308, doi:10.1029/91JD00198, 1991.

https://doi.org/10.5194/amt-2020-252
Preprint. Discussion started: 13 July 2020




Eisele, F. L. and Tanner, D. J.: Measurement of the gas phase concentration of H2SO4 and methane sulfonic acid and estimates of H2SO4 production and loss in the atmosphere, J. Geophys. Res., 98(D5), 9001–9010, doi:10.1029/93JD00031, 1993.

Fehsenfeld, F. C., Howard, C. J. and Schmeltekopf, A. L.: Gas phase ion chemistry of HNO3, J. Chem. Phys., 63(7), 2835–2841, doi:10.1063/1.431722, 1975.

Feiner, P. A., Brune, W. H., Miller, D. O., Zhang, L., Cohen, R. C., Romer, P. S., Goldstein, A. H., Keutsch, F. N., Skog, K. M., Wennberg, P. O., Nguyen, T. B., Teng, A. P., DeGouw, J., Koss, A., Wild, R. J., Brown, S. S., Guenther, A., Edgerton, E., Baumann, K. and Fry, J. L.: Testing atmospheric oxidation in an Alabama forest, J. Atmos. Sci., 73(12), 4699–4710, doi:10.1175/JAS-D-16-0044.1, 2016.

Fuchs, H., Dorn, H. P., Bachner, M., Bohn, B., Brauers, T., Gomm, S., Hofzumahaus, A., Holland, F., Nehr, S., Rohrer, F., Tillmann, R. and Wahner, A.: Comparison of OH concentration measurements by DOAS and LIF during SAPHIR chamber experiments at high OH reactivity and low NO concentration, Atmos. Meas. Tech., 5(7), 1611–1626, doi:10.5194/amt-5-1611-2012, 2012.

Heard, D. E. and Pilling, M. J.: Measurement of OH and HO2 in the Troposphere, Chem. Rev., 103(12), 5163–5198, doi:10.1021/cr020522s, 2003.

Hofzumahaus, A., Rohrer, F., Lu, K., Bohn, B., Brauers, T., Chang, C.-C., Fuchs, H., Holland, F., Kita, K., Kondo, Y., Li, X., Lou, S., Shao, M., Zeng, L., Wahner, A. and Zhang, Y.: Amplified Trace Gas Removal in the Troposphere, Science (80-. )., 324(5935), 1702–1704, doi:10.1126/science.1164566, 2009.

Holland, F., Hessling, M. and Hofzumahaus, A.: In situ measurement of tropospheric OH radicals by laser-induced fluorescence - a description of the KFA instrument, J. Atmos. Sci., 52(19), 3393–3401, doi:10.1175/1520-0469(1995)052<3393:ISMOTO>2.0.CO;2, 1995.

Kukui, A., Ancellet, G. and Le Bras, G.: Chemical ionisation mass spectrometer for measurements of OH and Peroxy radical concentrations in moderately polluted atmospheres, J. Atmos. Chem., 61(2), 133–154, doi:10.1007/s10874-009-9130-9, 2008.

Kulmala, M., Vehkamäki, H., Petäjä, T., Dal Maso, M., Lauri, A., Kerminen, V. M., Birmili, W. and McMurry, P. H.: Formation and growth rates of ultrafine atmospheric particles: A review of observations, J. Aerosol Sci., 35(2), 143–176, doi:10.1016/j.jaerosci.2003.10.003, 2004.

Kürten, A., Rondo, L., Ehrhart, S. and Curtius, J.: Calibration of a chemical ionization mass spectrometer for the measurement of gaseous sulfuric acid, J. Phys. Chem. A, 116(24), 6375–6386, doi:10.1021/jp212123n, 2012.

Lelieveld, J., Butler, T. M., Crowley, J. N., Dillon, T. J., Fischer, H., Ganzeveld, L., Harder, H., Lawrence, M. G., Martinez, M., Taraborrelli, D. and Williams, J.: Atmospheric oxidation capacity sustained by a tropical forest, Nature, 452(7188), 737–740, doi:10.1038/nature06870, 2008.

Levy, H.: Normal atmosphere: Large radical and formaldehyde concentrations predicted, Science (80-. )., 173(3992), 141–143, doi:10.1126/science.173.3992.141, 1971.

Liu, Y., Seco, R., Kim, S., Guenther, A. B., Goldstein, A. H., Keutsch, F. N., Springston, S. R., Watson, T. B., Artaxo, P., Souza, R. A. F., McKinney, K. A. and Martin, S. T.: Isoprene photo-oxidation products quantify the effect of pollution on hydroxyl radicals over Amazonia, Sci. Adv., 4(4), 1–9, doi:10.1126/sciadv.aar2547, 2018.

Lu, K. D., Rohrer, F., Holland, F., Fuchs, H., Bohn, B., Brauers, T., Chang, C. C., Häseler, R., Hu, M., Kita, K., Kondo, Y., Li, X., Lou, S. R., Nehr, S., Shao, M., Zeng, L. M., Wahner, A., Zhang, Y. H. and Hofzumahaus, A.: Observation and modelling of OH and HO2 concentrations in the Pearl River Delta 2006: A missing OH source in a VOC rich atmosphere, Atmos. Chem. Phys., 12(3), 1541–1569, doi:10.5194/acp-12-1541-2012, 2012.

https://doi.org/10.5194/amt-2020-252
Preprint. Discussion started: 13 July 2020




Lu, K., Guo, S., Tan, Z., Wang, H., Shang, D., Liu, Y., Li, X., Wu, Z., Hu, M. and Zhang, Y.: Exploring atmospheric free-radical chemistry in China: The self-cleansing capacity and the formation of secondary air pollution, Natl. Sci. Rev., 6(3), 579–594, doi:10.1093/nsr/nwy073, 2019.

Mao, J., Ren, X., Zhang, L., Van Duin, D. M., Cohen, R. C., Park, J. H., Goldstein, A. H., Paulot, F., Beaver, M. R., Crounse, J. D., Wennberg, P. O., Digangi, J. P., Henry, S. B., Keutsch, F. N., Park, C., Schade, G. W., Wolfe, G. M., Thornton, J. A. and Brune, W. H.: Insights into hydroxyl measurements and atmospheric oxidation in a California forest, Atmos. Chem. Phys., 12(17), 8009–8020, doi:10.5194/acp-12-8009-2012, 2012.

Mauldin, R. L., Frost, G. J., Chen, G., Tanner, D. J., Prevot, A. S. H., Davis, D. D. and Eisele, F. L.: OH measurements during the First Aerosol Characterization Experiment (ACE 1): Observations and model comparisons, J. Geophys. Res. Atmos., 103(D13), 16713–16729, doi:10.1029/98JD00882, 1998.

McKeen, S. A., Mount, G., Eisele, F., Williams, E., Harder, J., Goldan, P., Kuster, W., Liu, S. C., Baumann, K., Tanner, D., Fried, A., Sewell, S., Cantrell, C. and Shetter, R.: Photochemical modeling of hydroxyl and its relationship to other species during the Tropospheric OH Photochemistry Experiment, J. Geophys. Res. Atmos., 102(5), 6467–6493, doi:10.1029/96jd03322, 1997.

Novelli, A., Vereecken, L., Lelieveld, J. and Harder, H.: Direct observation of OH formation from stabilised Criegee intermediates, Phys. Chem. Chem. Phys., 16(37), 19941–19951, doi:10.1039/c4cp02719a, 2014.

Peeters, J., Nguyen, T. L. and Vereecken, L.: HOx radical regeneration in the oxidation of isoprene, Phys. Chem. Chem. Phys., 11(28), 5935–5939, doi:10.1039/b908511d, 2009.

Perner, D., Ehhalt, D. H., Pätz, H. W., Platt, U., Röth, E. P. and Volz, A.: OH - Radicals in the lower troposphere, Geophys. Res. Lett., 3(8), 466–468, doi:10.1029/GL003i008p00466, 1976.

Rohrer, F. and Berresheim, H.: Strong correlation between levels of tropospheric hydroxyl radicals and solar ultraviolet radiation, Nature, 442(7099), 184–187, doi:10.1038/nature04924, 2006.

Sjostedt, S. J., Huey, L. G., Tanner, D. J., Peischl, J., Chen, G., Dibb, J. E., Lefer, B., Hutterli, M. A., Beyersdorf, A. J., Blake, N. J., Blake, D. R., Sueper, D., Ryerson, T., Burkhart, J. and Stohl, A.: Observations of hydroxyl and the sum of peroxy radicals at Summit, Greenland during summer 2003, Atmos. Environ., 41(24), 5122–5137, doi:10.1016/j.atmosenv.2006.06.065, 2007.

Stone, D., Whalley, L. K. and Heard, D. E.: Tropospheric OH and HO2 radicals: Field measurements and model comparisons, Chem. Soc. Rev., 41(19), 6348–6404, doi:10.1039/c2cs35140d, 2012.

Tan, Z., Fuchs, H., Lu, K., Hofzumahaus, A., Bohn, B., Broch, S., Dong, H., Gomm, S., Häseler, R., He, L., Holland, F., Li, X., Liu, Y., Lu, S., Rohrer, F., Shao, M., Wang, B., Wang, M., Wu, Y., Zeng, L., Zhang, Y., Wahner, A. and Zhang, Y.: Radical chemistry at a rural site (Wangdu) in the North China Plain: Observation and model calculations of OH, HO2 and RO2 radicals, Atmos. Chem. Phys., 17(1), 663–690, doi:10.5194/acp-17-663-2017, 2017.

Tanner, D. J. and Eisele, F. L.: Present OH measurement limits and associated uncertainties, J. Geophys. Res., 100(D2), 2883–2892, doi:10.1029/94JD02609, 1995.

Tanner, D. J., Jefferson, A. and Eisele, F. L.: Selected ion chemical ionization mass spectrometric measurement of OH, J. Geophys. Res. Atmos., 102(5), 6415–6425, doi:10.1029/96jd03919, 1997.

Wang, T., Xue, L., Brimblecombe, P., Lam, Y. F., Li, L. and Zhang, L.: Ozone pollution in China: A review of concentrations, meteorological influences, chemical precursors, and effects, Sci. Total Environ., 575, 1582–1596, doi:10.1016/j.scitotenv.2016.10.081, 2017.

https://doi.org/10.5194/amt-2020-252
Preprint. Discussion started: 13 July 2020


Atmospheric Measurement Techniques Discussions

1 Wennberg, P. O., Stimpfle, R. M., Weinstock, E. M., Dessler, A. E., Lloyd, S. A., Lapson, L. B., Schwab, J.
2 J. and Anderson, J. G.: Simultaneous, in situ measurements of OH, HO2, O3, and H2O: A test of
3 modeled stratospheric HOx chemistry, Geophys. Res. Lett., 17(11), 1909–1912,
4 doi:10.1029/GL017i011p01909, 1990.

5 Whalley, L. K., Edwards, P. M., Furneaux, K. L., Goddard, A., Ingham, T., Evans, M. J., Stone, D., Hopkins,
6 J. R., Jones, C. E., Karunaharan, A., Lee, J. D., Lewis, A. C., Monks, P. S., Moller, S. J. and Heard, D. E.:
7 Quantifying the magnitude of a missing hydroxyl radical source in a tropical rainforest, Atmos. Chem.
8 Phys., 11(14), 7223–7233, doi:10.5194/acp-11-7223-2011, 2011.

9

https://doi.org/10.5194/amt-2020-252
Preprint. Discussion started: 13 July 2020


Atmospheric Measurement Techniques Discussions

## Figures

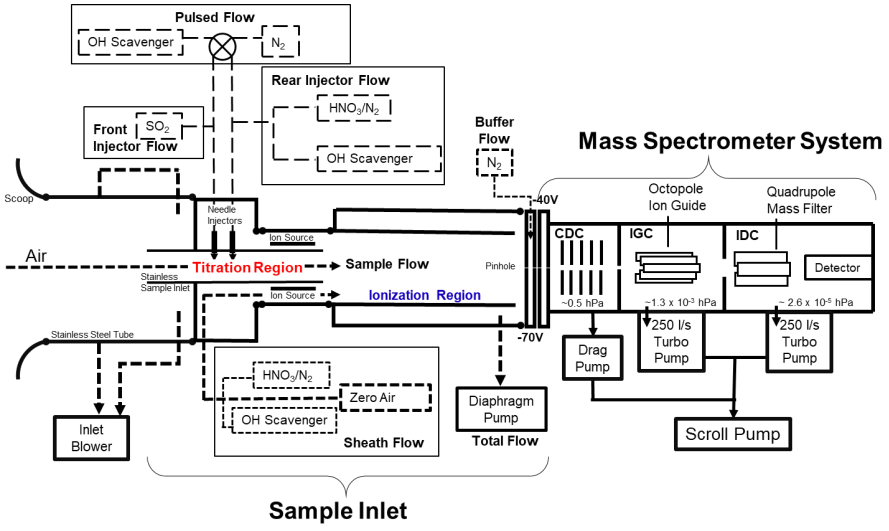


**Figure 1**. Schematic diagram of the OH-CIMS system, which including a sample inlet system and a mass spectrometer system. The sample inlet system including chemical titration region and chemical ionization region. The mass spectrometer system consists by a collisional dissociation chamber (CDC), an ion guide chamber (IGC), and an ion detection chamber (IDC). Dashed lines depict the air flows in the sample inlet during operations.

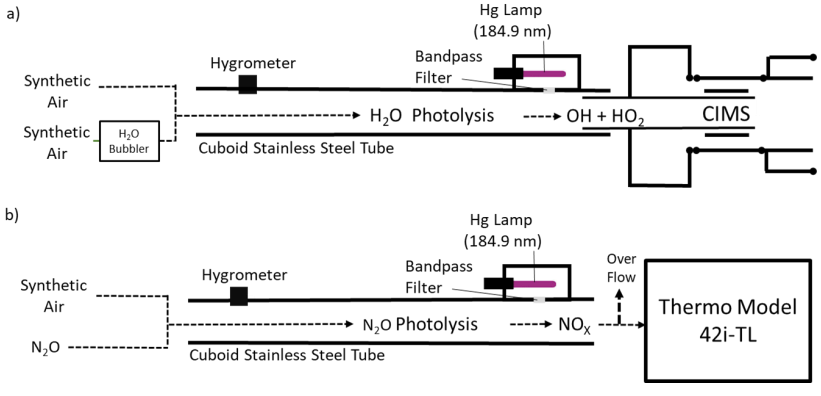


**Figure 2.** Schematic diagram of calibration. a) The CIMS calibration experiment. b) The $N_2O$ actinometry experiment for determination of product *It* value. Dashed lines show the air flows during experiment.

https://doi.org/10.5194/amt-2020-252
Preprint. Discussion started: 13 July 2020


Atmospheric Measurement Techniques Discussions

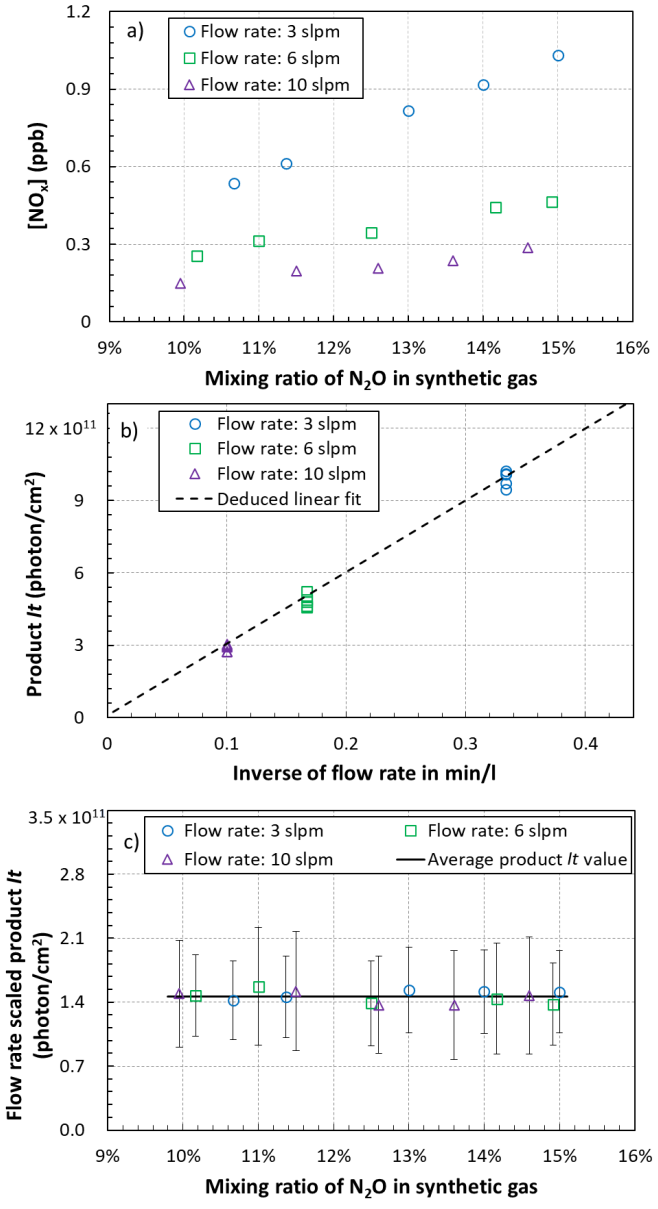


**Figure 3.** The results of $N_2O$ actinometry experiment. a) The produced $NO_x$ concentration as a function of $N_2O$ mixing ratio. Different colors represent different flow rates. b) The product *It* as a function of inverse of flow rate (see detail in text). c) The flow rate scaled product *It* as a function of $N_2O$ mixing ratio, which was obtained by scaling product *It* with the ratio of flow rates (3, 6, and 10 slpm) to 10 slpm. Black line is the average value of flow rate scaled product *It*. The error bars represent uncertainties ($2\sigma$) for flow rate scaled product *It*. The average uncertainty of the product *It* is 36%.

https://doi.org/10.5194/amt-2020-252
Preprint. Discussion started: 13 July 2020


Atmospheric Measurement Techniques Discussions

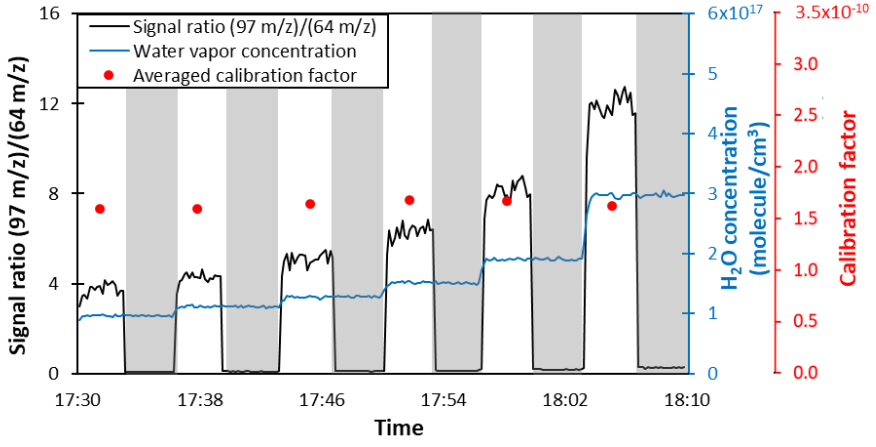


**Figure 4.** The time series showing calibration result. Gray labeled areas represent the background mode during calibration. Black line represents the ratio of signal intensity at 97 m/z and 64 m/z. Blue line represents water vapor concentration. Red dots represent the 3-minute averaged calibration factors at different steps.

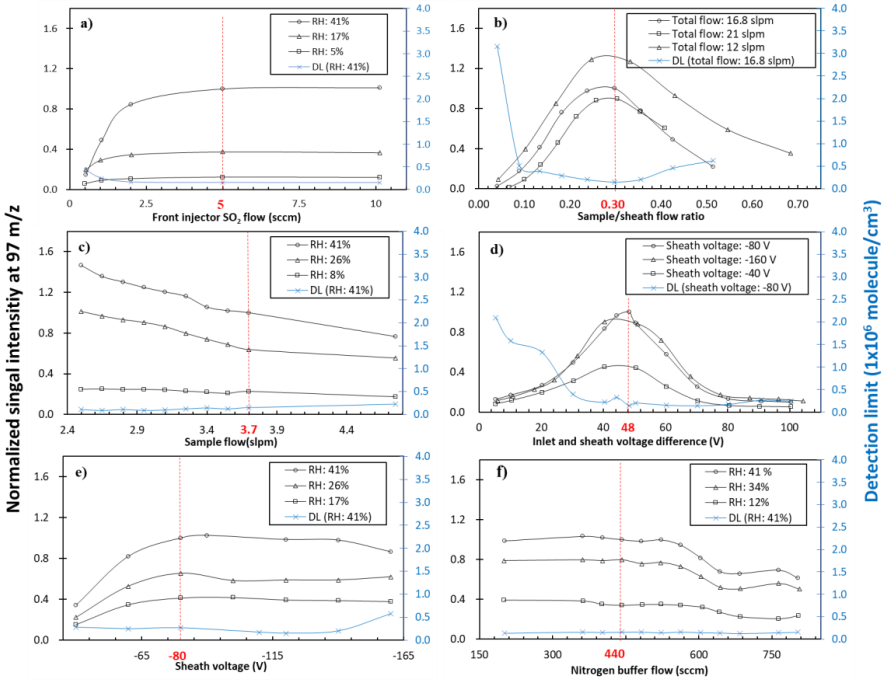

https://doi.org/10.5194/amt-2020-252
Preprint. Discussion started: 13 July 2020


Atmospheric Measurement Techniques Discussions

**Figure 5.** The normalized signal intensity at 97 m/z and detection limit as a function of a) $SO_2$ flow rate b) sample/sheath flow ratio, c) sample flow with fixed sample/sheath flow ratio, d) inlet and sheath voltages difference, e) sheath voltage with fixed voltage difference between inlet and sheath voltages, f) $N_2$ buffer flow with the other parameters constant. The signal is normalized based on the signal intensity at the settings of 5 sccm $SO_2$, 16.8 slpm total flow, 12.6 slpm sheath flow, 3.7 slpm sample flow, 440 sccm $N_2$ buffer flow, -80V sheath voltage, -32 V inlet voltage, and 41% relative humidity of the sample air. Red dashed lines highlight the optimized values selected for our CIMS.

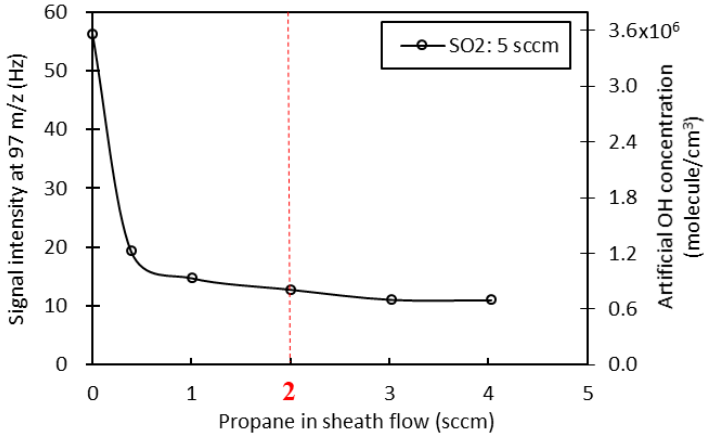


**Figure 6.** Artificial OH signal as a function of propane flow rate added in sheath flow. N2 gas was used as sample air so that there were no OH radicals in sample air. Red dashed line was the optimized flow rate applied for our CIMS.

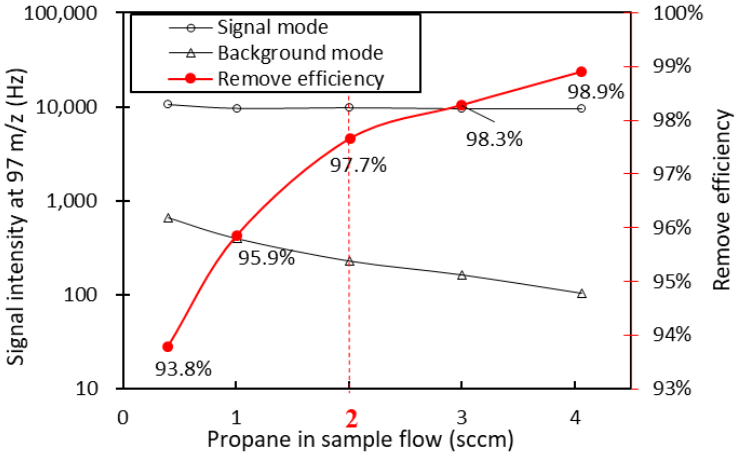


**Figure 7.** Signal intensity at 97 m/z and OH remove efficiency as a function of propane flow rate added in the sample flow propane during the calibration experiment. The relative humidity of sample air was 41%. $SO_2$ flow rate was 5 sccm. Red dashed line highlights the optimized flow rate applied for our CIMS.

https://doi.org/10.5194/amt-2020-252
Preprint. Discussion started: 13 July 2020


Atmospheric Measurement Techniques Discussions

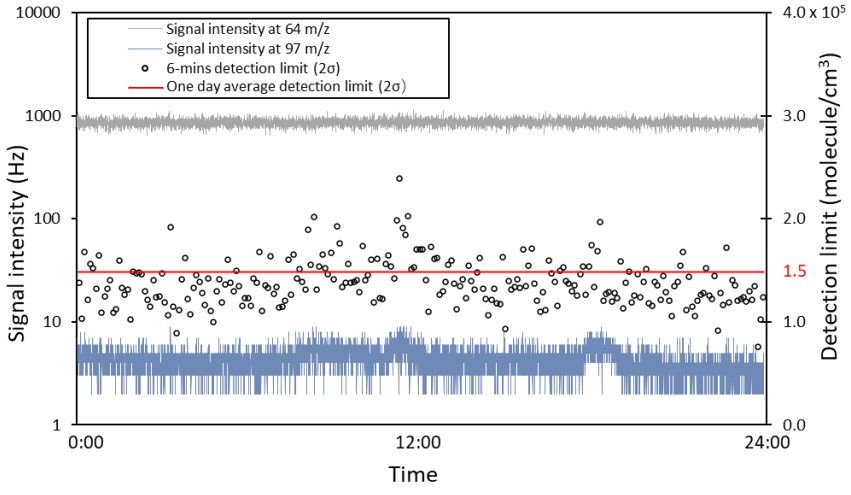


**Figure 8.** The detection limit (2σ) of the CIMS. One day averaged detection limit is $1.5 \times 10^5$ molecule/$cm^3$.

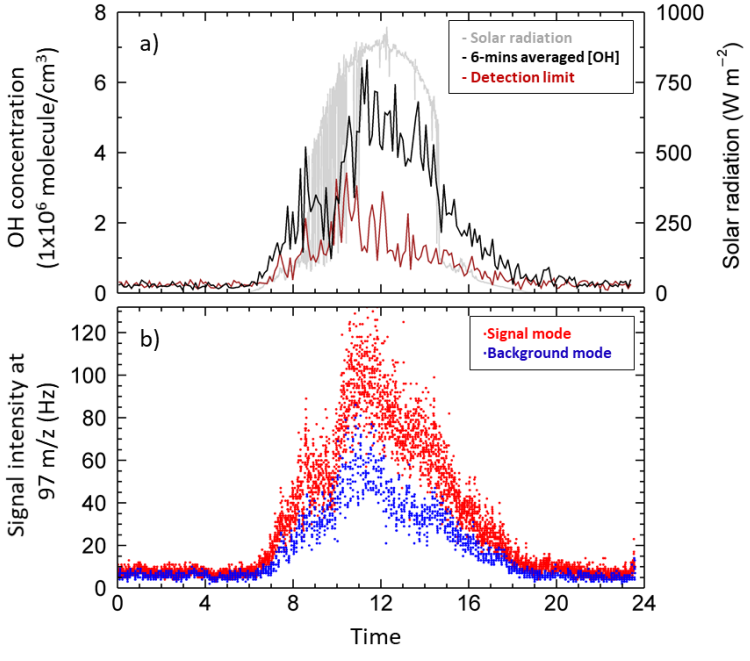


**Figure 9.** a) Diurnal variation of OH concentration and solar radiation on the 11th floor of a teaching building on the campus of the Hong Kong Polytechnic University on April 25, 2019. b) The signal intensity at 97 m/z for two different measurement modes.